Geophysical Research Letters

RESEARCH LETTER
10.1029/2023GL105664

Northern Hemisphere Summer Insolation and Ice Volume Driven Variations in Hydrological Environment in Southwest China

Yao Wu[1], Sophie Warken[1], Norbert Frank[1], Aaron Mielke[1], Chao-Jun Chen[2], Jun-Yun Li[3], and Ting-Yong Li[2]

[1]Institute of Environmental Physics, Heidelberg University, Heidelberg, Germany, [2]Yunnan Key Laboratory of Plateau Geographical Processes & Environmental Changes, Faculty of Geography, Yunnan Normal University, Kunming, China, [3]Chongqing Key Laboratory of Karst Environment, School of Geographical Sciences, Southwest University, Chongqing, China

Key Points:

- Stalagmite trace elements are indicators of regional hydrological environmental variations in Southwestern China
- Northern Hemisphere summer insolation and global ice volume modulate the phase and amplitude variations of regional hydrological environment
- The meridional tripolar spatial pattern of precipitation in monsoon region in China on the orbital scale remains ambiguous

Supporting Information:

Supporting Information may be found in the online version of this article.

Correspondence to:

Y. Wu and T.-Y. Li,
ywu@iup.uni-heidelberg.de;
cdlty@163.com

Citation:

Wu, Y., Warken, S., Frank, N., Mielke, A., Chen, C.-J., Li, J.-Y., & Li, T.-Y. (2023). Northern Hemisphere summer insolation and ice volume driven variations in hydrological environment in southwest China. *Geophysical Research Letters*, *50*, e2023GL105664. https://doi.org/10.1029/2023GL105664

Received 16 OCT 2023
Accepted 9 NOV 2023

Author Contributions:

Conceptualization: Yao Wu, Sophie Warken, Norbert Frank, Ting-Yong Li
Data curation: Yao Wu, Sophie Warken, Aaron Mielke
Funding acquisition: Norbert Frank, Ting-Yong Li
Investigation: Chao-Jun Chen, Jun-Yun Li
Writing – original draft: Yao Wu
Writing – review & editing: Sophie Warken, Norbert Frank, Ting-Yong Li

Abstract The interpretation of stalagmite $\delta^{18}O$ in terms of reflecting Asian summer monsoon (ASM) precipitation is still elusive. Here, we present high-resolution stalagmite trace element ratios (X/Ca, X = Mg, Sr, Ba) records from southwest China covering 116.09 to 4.07 ka BP. $\delta^{18}O$, $\delta^{13}C$, and X/Ca values exhibit clear precessional cycles, with $\delta^{18}O$ values reflecting ASM circulation/intensity, while X/Ca ratios capture local precipitation or evapotranspiration variations. Our results show that Northern Hemisphere summer insolation (NHSI) is the main driver of ASM intensity and precipitation phase variation, but global ice volume modulates the response magnitude of summer precipitation to insolation. During the Last Glacial Maximum, high ice volumes caused significant monsoon precipitation to decrease. In contrast to modern observations of the tripolar distribution of precipitation in China, our record is consistent with paleo-precipitation records in southern and northern China.

Plain Language Summary While it is well known that global changes have led to variations in the intensity and spatial distribution of Asian monsoon precipitation, the mechanisms behind this are not well understood. Paleoclimate records are essential for revealing the drivers behind monsoon variation. However, speleothem records from the Asian monsoon region rarely provide direct information on the amount of rainfall. Here we report on multiple indicator data sets from a stalagmite in southwestern China. It could help explore the variation of monsoon precipitation over the last ~100,000 years. We find that the increase/decrease of Northern Hemisphere summer insolation controls the increase/decrease of Asian summer monsoon rainfall. In addition, global ice volume moderates the magnitude of rainfall response to insolation, and precipitation decreases significantly during high ice volume periods. Based on the present paleo-precipitation records evidence, the existence of the spatial pattern of increasing/decreasing rainfall in central China corresponding to decreasing/increasing rainfall in northern and southern China remains ambiguous on the orbital scales, although the feature has been captured by some of the model simulations.

1. Introduction

Oxygen isotope measurements in speleothem carbonate ($\delta^{18}Oc$) from the Asian monsoon region provide valuable climatic information for exploring of the driving mechanisms, the evolutionary processes, and intensity of the late Quaternary Asian summer monsoon (ASM) (Cheng et al., 2016, 2019). This concept encompasses several aspects of the ASM system, such as changes in moisture source and shifts in circulation patterns (Maher & Thompson, 2012; M. Tan, 2014), upstream Rayleigh fractionation (Hu et al., 2008), summer to winter precipitation ratio (Wang et al., 2001), and the variations in ASM circulation intensity or overall precipitation (Cheng et al., 2019). The interpretation of $\delta^{18}Oc$ as an indicator of local rainfall amount in the monsoon region in China remains, however, controversial (e.g., Lachniet, 2020; Liu et al., 2020; Xue et al., 2023). For only a few of the $\delta^{18}Oc$ records in China a correlation with local amount of precipitation was demonstrated (Liu et al., 2008; L. C. Tan et al., 2014, 2015), while a relationship with the local instrumental rainfall record is often lacking (Xue et al., 2023; Yang et al., 2019). $\delta^{18}Oc$ may also be related to the strength of the large-scale atmospheric circulation and moisture transport, instead of providing direct measures of the regional precipitation quantity (Cheng et al., 2019; Liu et al., 2014).

There is significant spatial heterogeneity in precipitation across the monsoon region in China. In the modern era and the Holocene, precipitation in central China exhibits an inverse phase within southern and northern China. The increased rainfall in central China corresponds to a decrease in southern and northern China, also known as the "tripolar" pattern (Figure S1 in Supporting Information S1) (Chen et al., 2022; Chiang et al., 2017; Zhang et al., 2018). This pattern is difficult to observe in the δ^{18}Oc records from the monsoon region in China because dynamical elements are not sufficiently well-constrained, limiting the ability of δ^{18}Oc to capture the ASM thermodynamic nature and the rainfall amount (Zhao, Cheng, et al., 2023). In respect to the driving mechanisms, compared to the ASM rhythms primarily controlled by Northern Hemisphere summer insolation (NHSI) (Cheng et al., 2016, 2021), the response of China summer precipitation to astronomical forcing and ice volume appears elusive. For example, summer precipitation in northern China is controlled by precession, showing significant 23 ka cycles, while in southern China 100 ka cycles are well present, indicating the dominant influence of the background climate state as for example, represented by the global ice volume (Dai et al., 2021; Lyu et al., 2021; Zhao, Lu, et al., 2023). In addition to NHSI and ice volume, it has also been hypothesized that the ASM is primarily driven by the Summer Inter-Tropical Insolation Gradient (SITIG) (Cheng et al., 2022; Zhang et al., 2023). During the precessional minima (P_{min}), the increase in SITIG leads to a more pronounced northward shift of the Intertropical convergence zone (ITCZ) and enhanced western Pacific subtropical high and winter hemisphere trans-equatorial Hadley circulation (Beck et al., 2018). It eventually transports more oceanic moisture and latent heat to the Asian monsoon continent. This perspective emphasizes the "pull" and "push" forcing of ASM variations by inter-hemispheric temperature gradients, which is a more comprehensive theory than the traditional single factor driven view of ASM evolution (Cheng et al., 2022). The discussion of the relationship between ASM and spatial heterogeneity in summer precipitation has focused on the Holocene, or millennial events of the last glacial period. On longer scales there is a heavy reliance on simulations (Dai et al., 2021; Lyu et al., 2021). Due to the absence of high-resolution precipitation reconstructions on glacial-interglacial periods, the existence of spatial precipitation heterogeneity and its forcing factors remain unclear for at orbital time scales.

Another aspect of our work is that the relationship between regional hydrological environment wet-dry variation and ASM intensity may not remain constant over different times scales. During the millennial-scale climate events of the Last Glacial Maximum (LGM), the Yangtze River basin in central China experienced wet conditions during Heinrich event (H) 1 and Younger Dryas, although the ASM weakened significantly (Zhang et al., 2018). In contrast, the environment in the central Yangtze basin was dry and cold during H5 and H6, while it was wet and warm during Greenland Interstadials (GI) 9–18 (Wang, Chen, et al., 2022). In southwest China, the regional hydrological environment and effective rainfall during H4 and H5 were comparable to or even wetter than GIs (Liu et al., 2022; Wu et al., 2023). In summary, δ^{18}Oc does not necessarily indicate regional precipitation variations, as circulation or moisture source effects may mask the less dominant local precipitation signals.

Currently, there are very few unambiguous regional rainfall or hydrological environment records spanning the glacial-interglacial cycle in southern China, with a resolution permitting to investigate individual millennial climate events. But some recent work has attempted to reconcile the relationship between ASM intensity and precipitation from the simulation perspective (Dai et al., 2021; Lyu et al., 2021; Zhao, Lu, et al., 2023). Here we report trace element records (Mg/Ca, Sr/Ca, Ba/Ca) for a stalagmite from Yangzi cave in southwest China spanning 116.09 to 4.07 ka BP. In combination with δ^{18}Oc and δ^{13}Cc values, this record provides much clearer comparisons for assessing the relationship between ASM intensity and the regional hydrological environment.

2. Material and Methods

2.1. Study Area and Sample

Yangzi cave (29.78°N, 107.78°E, 400 m above sea level) is located on the lower reaches of Longhe River, which is a tributary of Yangtze River in Fengdu County, Chongqing City, southwestern China (Figure S1 in Supporting Information S1). Yangzi cave is about 500 m long, developed in lower Triassic limestone (Zhu et al., 2004). The region has a subtropical humid monsoon climate, which is affected by the ASM (Pu et al., 2015). Instrumental climate data from the nearest meteorological station (18 km northwest of Yangzi Cave), reveal that the mean annual temperature and precipitation amount are 18.3°C and 1018.6 mm, and the 1980–2010 averages June-October precipitation accounts for 70% of the entire year (http://www.cma.gov.cn/). The mean cave temperature is approximately constant at 16.0°C, and the humidity is close to 100% (Zhu et al., 2004). The modern vegetation above Yangzi cave primarily consists of subtropical perennial broad-leaved forests and shrubs (Pu et al., 2015). Details of the YZ1 stalagmite are described in Wu et al. (2020) and Text S1 in Supporting Information S1.

2.2. Methods

The analytical setup and measurement protocol of trace elements follows the method described by Warken et al. (2021). The analysis of trace elements was performed at the Institute of Environmental Physics, Heidelberg University. A laser ablation system with a 193 nm ArF excimer laser (NWR193UC by New Wave Research) was used to ablate carbonate, which was analyzed for its major and trace element composition using an inductively coupled plasma quadrupole mass spectrometer (ICPMS) (Thermo Fisher iCAP-Q). Line scans were performed at a speed of 10 µm/s along the growth axis of YZ1 with a rectangular spot size of 15 × 150 µm. To remove possible surface contamination, the scan path was pre-ablated at a scan speed of 80 µm/s. The repetition rate of the laser pulses was 20 Hz, and each investigated isotope was measured every 100 ms on the mass spectrometer. Background counts were measured with the laser in off mode and subtracted from the raw data. To account for matrix effects, the blank corrected count rates of the analyzed isotopes (^{25}Mg, ^{88}Sr, ^{138}Ba) are calculated relative to the intensity of ^{43}Ca. The silicate glass NIST SRM 612 was analyzed for external calibration of the trace element to Ca ratios using the reference values by Jochum et al. (2011). Correlation analyses were performed in SPSS 25 software. Principal component analysis was performed in R. Ensemble empirical mode decomposition (EEMD), bandpass filters, and spectral analysis were performed on MATLAB 2022b platform.

3. Results

Measurement results for stalagmite trace element ratios (Sr/Ca, Mg/Ca and Ba/Ca; in the following referred to as X/Ca) are presented in g/g and shown in Figure S2 in Supporting Information S1. The results of the Pearson correlation statistics revealed robust correlation coefficients between X/Ca of $0.46 < r < 0.75$ ($p < 0.01$) (Figure S3 in Supporting Information S1). Principal component analysis showed that totals of 76% and 18% of the variations in X/Ca data were explained by the first and second principal components (PCs) (Table S1 in Supporting Information S1). The results of the EEMD analyses suggests that the most relevant variability of X/Ca PC1 is captured by the component (IMF 7) that is coincident with precessional cycles (~23 ka) (Figure S4 and Table S2 in Supporting Information S1). On the orbital scale, X/Ca share substantial in-phase covariation to the oscillatory variations of δ^{18}O and δ^{13}C, as reflected by the highly significant Pearson correlation coefficients ($0.23 < r < 0.53$, $p < 0.01$) (Figure S3 in Supporting Information S1). The values of X/Ca are generally elevated compared to the mean value during MIS5e, MIS5c, MIS4 and MIS2, and overall lower during MIS3 (Figure S2 in Supporting Information S1).

4. Discussion

4.1. Climatic Significance of the Trace Element Ratios

The differential increase in the relative content of trace elements in stalagmites and positive correlation between all three elements was interpreted as prior calcite precipitation (PCP) (Fairchild et al., 2006; Shi et al., 2022; Stoll et al., 2022; Warken et al., 2018). Sinclair, Wassenburg, and their co-workers infer that predominance of PCP can be tested d through linear regression between ln(Sr/Ca) and ln(Mg/Ca) (Sinclair et al., 2012; Wassenburg et al., 2020). Here, the slopes of 1.0–1.2 between elemental ratios agree with model predictions (0.7–1.4) (Figure S5 in Supporting Information S1). During MIS5e and LGM, values of Mg/Ca and Sr/Ca are similar, while Sr/Ca is elevated in MIS5d (Figure S2 in Supporting Information S1). This difference may reflect the partitioning coefficient dependencies for Mg and Sr during calcite growth (D(Mg) and (D(Sr)) (Text S2 in Supporting Information S1), including dependence on saturation state of drip water, cave P_{CO2}, and temperature. The D(Mg) increased with increasing temperature (Fairchild et al., 2006), whereas the D(Sr) is positively correlated with stalagmite growth rate and may be controlled by solution saturation under the influence of cave ventilation (Day & Henderson, 2013). During the LGM, lower temperatures may result in lower D(Mg), which contradict our findings (Figure S2 in Supporting Information S1). Although higher stalagmite growth rates lead to significant increases in D(Sr), we do not find a positive offset during the LGM with twice as high growth rates during MIS5e (Figure S2 in Supporting Information S1). There is, however, solely an effect on D(Sr) when growth rates are greater than 315 mm/ka (Gabitov et al., 2014), which is much lower for YZ1. In addition, the relative stable Sr/Mg ratios of YZ1 further suggest that both elements have common and relatively constant source to the drip water during bedrock weathering. Tremaine and Froelich propose to use the Mg/Ca and Sr/Ca ratio under such conditions as indicator of rainfall variation (Tremaine & Froelich, 2013). Therefore, we consider that factors

such as temperature, growth rate are less likely to be the dominant factors controlling changes in trace elements compared to the strong indication for PCP.

Compared to Mg/Ca and Sr/Ca, Ba/Ca shows a low mean value of 0.04×10^{-3} but the variability is largest with variations of more than 500% (Figure S2 in Supporting Information S1). Hence, the variability and concentration of Mg, Sr, Ba follows inverse order with Mg/Ca > Sr/Ca > Ba/Ca and vice versa. We consider that Ba/Ca is probably the most sensitive indicator of response to PCP. Given the strong synchronicity of the three trace element ratios on orbital-millennial time scales, and to avoid the uncertainties of using single trace element ratio record, we use PC 1 of the X/Ca time series as a robust, integrated hydroclimatic record, interpreted as the local precipitation amount or evapotranspiration variations. The high variance of PC1 (76%) means that it well identifies the main patterns of variation in the X/Ca. The lower X/Ca PC1 values indicate wetter conditions and vice versa for drier conditions.

We compare X/Ca PC1 with δ^{13}Cc and U concentrations from stalagmite chronology results to further validate our interpretation. δ^{13}Cc and U concentrations are also considered sensitive indicators of response to the external hydrological environment (Fohlmeister et al., 2020; Jamieson et al., 2016). Additionally, X/Ca PC1 reveals similar trends throughout those of δ^{13}Cc and U concentration on orbital time scale (Figure S2 in Supporting Information S1). The extensive synchronisation of these multi-indicator records on orbital scales supports our interpretation of X/Ca PC1 as an indicator of regional hydroclimatic variations. Since the underlying PCP process is a non-linear Rayleigh process, we also use $\frac{Mg/Ca_{min}}{Mg/Ca_{sample}}$ to approximate the remaining fraction f_{Ca} in the drip water, which may serve as a more linear, that is, more direct proxy for regional precipitation amount variation than the X/Ca ratios (Stoll et al., 2022, Figure S6 and Text S2 in Supporting Information S1).

4.2. Precessional Forcing of the Regional Hydrological Environment

During MIS2, MIS4 and MIS5c with lower-than-average NHSI, the positive shifted δ^{18}Oc indicate the significant weakening of ASM intensity (Figure 1). Meanwhile, the higher δ^{13}Cc and X/Ca PC1 values associated with lower f_{Ca} values (Figure 1; Figure S6 in Supporting Information S1) suggest substantial deterioration in the regional vegetation and soil carbon dynamics, and precipitation. Such changes may reflect the degradation of the hydrological environment forced by the weakening ASM in southwest China, including decreased temperature, drought, and changes in the ratio of C3/C4 plants (Fohlmeister et al., 2020; Tremaine & Froelich, 2013). Although the relative contribution of each factor is difficult to determine, this ratio captures the combined impact of environmental degradation. During periods of above-average NHSI, that is, MIS1, MIS3, and MIS5a, the opposite of the low NHSI periods was observed, with lower δ^{13}Cc and X/Ca PC1 values as well as higher f_{Ca} values (Figure 2). This implies that NHSI not only triggers variations in ASM intensity, but also controls local precipitation variations. Strong NHSI corresponds to stronger ASM circulation and thus enhanced monsoon-related precipitation as compared to periods of weaker NHSI. The EEMD and spectral analysis also confirms that the precession cycle is significant in both the X/Ca PC1 and f_{Ca} records (Figures S4 and S6 in Supporting Information S1). Recent precipitation simulations for the past 300 ka BP in northern China also show significant precession influence, highlighting the dominant role of insolation (Zhao, Lu, et al., 2023). Similar results are confirmed in the magnetic susceptibility record from lake sediments in southern China (Wang, Lu, et al., 2022). Our trace element-derived precipitation reconstruction from southwest China, now provides a continuous record even during the low NHSI (Figure 1b).

The stalagmite δ^{13}Cc values in Zhenzhu cave from northern China are considered a sensitive indicator of response to variation in local precipitation (Figure 1c) (Y. X. Li et al., 2020). Zhenzhu Cave is in the monsoon edge region of northern China, which is most sensitive to ASM variations. Zhenzhu cave stalagmite halted growth during the periods of lowest solar insolation (MIS2, MIS4, MIS5b, and MIS5d), which we interpret as extreme weakening of the ASM, leading to a remarkable reduction in summer rainfall brought about by the southward retreat of the monsoon. This interpretation does not conflict with the insolation driven changes in ASM intensity and precipitation.

4.3. Low-Latitude Insolation Regulates Orbital-Scale ASM Precipitation

To assess the influence of forcing from low latitudes on ASM variation, we use the June 21 insolation difference between 30°N and 30°S to indicate variation in the Summer Inter-Tropical Insolation Gradient (SITIG). Our

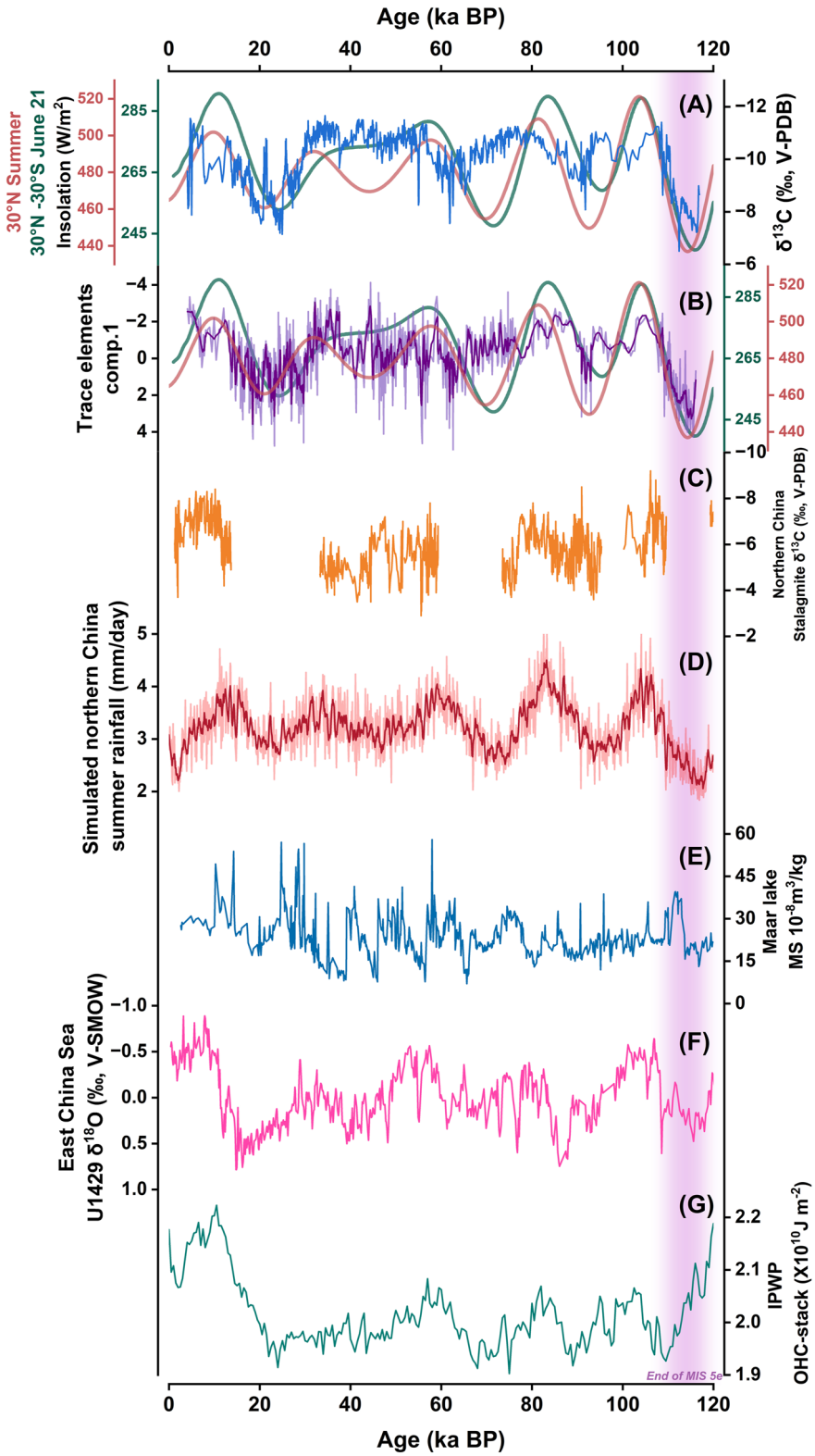

Figure 1. The YZ1 $\delta^{13}C$ and X/Ca PC1 records compared with climatic records for the Asian monsoon region. (a) YZ1 $\delta^{13}C$ (this study); (b) YZ1 X/Ca PC1 (this study), the dark curve indicates 10-points smoothing; (c) Zhenzhu Cave stalagmite $\delta^{13}C$ (Y. X. Li et al., 2020); (d) Summer rainfall in northern China as simulated by the full coupled NRAR-CCSM3 model (Zhao, Lu, et al., 2023); (e) Maar lake sediments Magnetic susceptibility (Wang, Lu, et al., 2022); (f) IODP U1429 planktonic foraminifer $\delta^{18}O$ (Clemens et al., 2018); (g) Indo-Pacific Warm Pool upper stacks ocean heat content variations (Jian et al., 2022). The brown and green curves represent 30°N summer and 30°N minus 30°S June 21 insolation, respectively (Laskar et al., 2004).

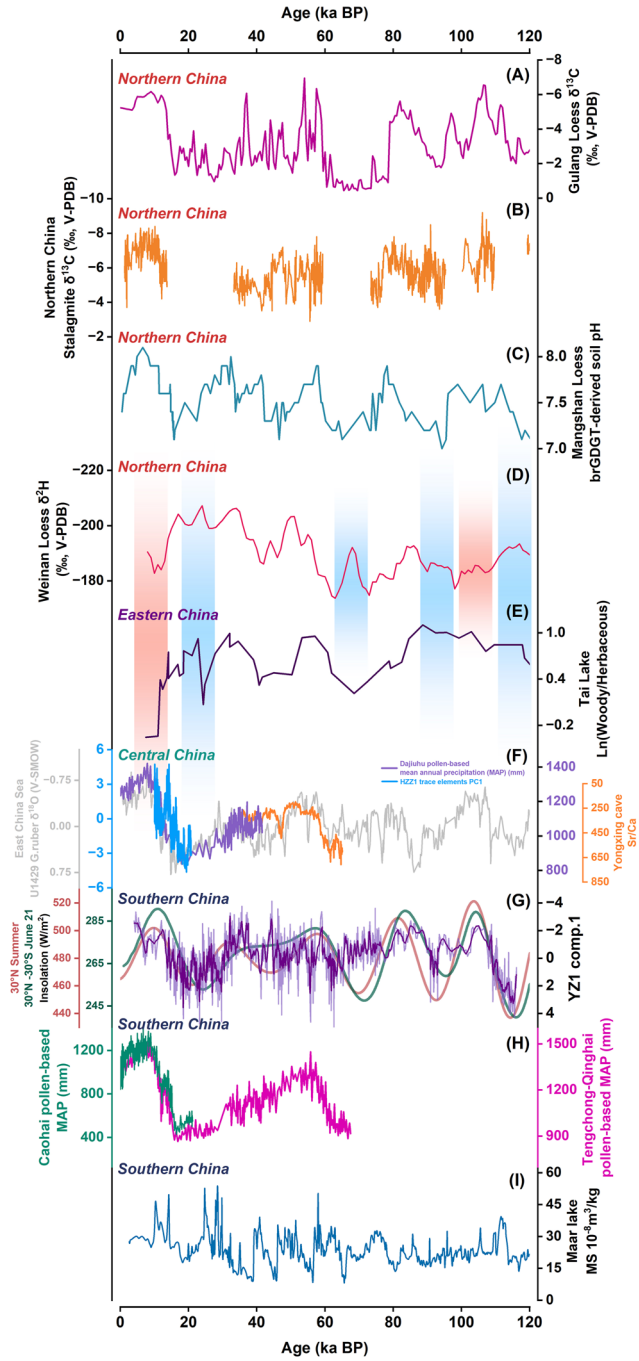

Figure 2. Comparison of the YZ1 X/Ca records with paleoclimate records from different regions of China. (a) Gulang loess $\delta^{13}C$ (Sun et al., 2015); (b) Zhenzhu Cave stalagmite $\delta^{13}C$ (Y. X. Li et al., 2020); (c) Mangshan loess brGDGT-derived soil pH (Peterse et al., 2014); (d) Weinan loess $\delta^{2}H$ (Thomas et al., 2016); (e) Tai Lake pollen ratio of Woody/Herbaceous (Miao et al., 2015); (f) IODP U1429 planktonic foraminifer $\delta^{18}O$ (gray) (Clemens et al., 2018); Haozhu cave stalagmite trace elements PC1 (bule) (Zhang et al., 2018); Dajiuhu pollen-based mean annual precipitation (purple) (Zhang et al., 2023); Yongxing cave stalagmite Sr/Ca (orange) (Wang, Chen, et al., 2022); (g) YZ1 X/Ca PC1 (this study); (h) Pollen-based MAP records of Caohai (green) and Tengchong-Qinghai (pink), respectively (Zhang et al., 2023); (i) Maar lake sediments Magnetic susceptibility (Wang, Lu, et al., 2022). The red/blue bars indicate paleoclimatic records where increased/decreased insolation corresponds to decreased/increased precipitation.

reconstructed precipitation variations point to a link with SITIG (Figure 1). Although, the NHSI and SITIG are nearly identical in phase, the decreasing NHSI is contrasting the elevated precipitation during MIS3, which is synchronous to SITIG (Figure 1). This finding supports the fact that inter-hemispheric heat contrasts also cause ASM precipitation variation (Beck et al., 2018; Zhang et al., 2023). To validate this forcing, we compared our X/Ca PC1 record with marine proxies from ASM moisture source region (Figures 1b and 1g). The Indo-Pacific Warm Pool (IPWP) upper ocean heat content (OHC) variations exhibit significant precession cycles driven by the insolation-driven meridional gradients in the lower latitudes (Figure 1g) (Jian et al., 2022). The OHC and YZ1 $\delta^{18}O$ and X/Ca PC1 are in phase on the precession scale. This could be explained by the ASM dynamics and thermodynamics are influenced by the tropics warm pool ocean heat content. The increase in IPWP OHC during P_{min} results in more evaporation, convergence, and transport of oceanic moisture to land (Jian et al., 2022). This process, while increasing East Asian monsoon precipitation, also produces more depleted $\delta^{18}O$ values in the speleothem records due to significant upstream moisture convergence and rainout (Figures 1a, 1b, and 1g) (Liu et al., 2014; Ruan et al., 2019). The above phenomena and processes have been confirmed in quantitatively reconstructed precipitation records on orbital scales based on pollen in southern China and loess in the north China (Beck et al., 2018; Zhang et al., 2023). For the first time, we observe similar features in stalagmite trace element records from southern China. Our new record highlights that differences in insolation between the low-latitude tropics may be a more integrated forcing factor controlling monsoon precipitation phase variations (Cheng et al., 2022).

Simulations have suggested that the "tripolar" precipitation pattern in the monsoon region of China during the modern and Holocene persists on orbital scales (Figure S7 in Supporting Information S1) (Dai et al., 2021; Lyu et al., 2021). However, our findings are broadly consistent with precipitation reconstructions in northern and southern China, that is, wet environments correspond to high NHSI or large SITIG, although there are differences in details (Figure 2). We observed antiphase only in loess $\delta^{2}H$ records near the edge of the Loess Plateau and in Taihu lake pollen proxies in the lower reaches of the Yangtze River (Figures 2d and 2e). These records show that the decrease in insolation sometimes corresponds to a wetter environment. The spatial heterogeneity of precipitation in the monsoon region in China is often interpreted as being related to Western Pacific Subtropical High (WPSH) (Chiang et al., 2017; Jiang et al., 2021). During high boreal summer insolation, a more La Niña-like state caused by the increased tropical east-west Pacific Sea surface temperature gradient will result in stronger and more active WPSH (N. N. Li et al., 2021; Lu et al., 2019). Enhanced and northwardly extending WPSH limits summer precipitation in east-central China while precipitation increases in north and south China (Zhang et al., 2020). However, there is also evidence that strong WPSH can also lead to an east-west antiphase of summer precipitation in the mid-latitude monsoon region in China (Tian et al., 2022). Our results show high NHSI and La Niña-like situations correspond to increased precipitation (Figure S8 in Supporting Information S1). Moreover, we also do not find similar antiphase in U1429 $\delta^{18}O$ indicative of the overall rainfall in the Yangtze River basin (Figure 2) (Clemens et al., 2018), suggesting that the generalized statement that central China is in antiphase with north-south precipitation may not be robust. The typical areas where high NHSI corresponds to negative precipitation anomalies are in the middle and lower reaches of the Yangtze River, which are more affected by WPSH (Dai et al., 2021; Jiang et al., 2021). The absence of continuous paleo precipitation records spanning the glacial-interglacial period in the middle and lower reaches of the Yangtze River also creates uncertainty in the interpretation (Figure S7 in Supporting Information S1). Therefore, its influencing range should be considered when discussing the spatial patterns of precipitation in the monsoon region in China on orbital scales. Also, caution should be exercised when discussing monsoon precipitation variations based on a single reconstructed record.

4.4. The Global Ice Volume Forcing on Summer Monsoon Precipitation Amplitudes

The band bass filter analysis results show a long-term decreasing trend in $\delta^{18}Oc$ from MIS5e to MIS1, with the phase and amplitude consistent with the precession (Figure 3). However, during the LGM, although the X/Ca PC1 record is in phase with the ASM and insolation, the amplitude is much larger, equivalent to strongly decreasing precipitation amounts as deduced from f_{Ca} estimates (Figure S6 in Supporting Information S1). Similar results are confirmed in different model simulations. The LGM annual precipitation in China was proposed to reduce by an average of 18%–25% compared to the pre-industrial period (Tian & Jiang, 2016). This suggests that the decrease in ASM precipitation during the LGM is exceeding the influence of ASM intensity, which is also captured by other precipitation records (Figure 3). The forcing of the intensely reduced precipitation during the LGM is not completely attributable to the decreasing insolation.

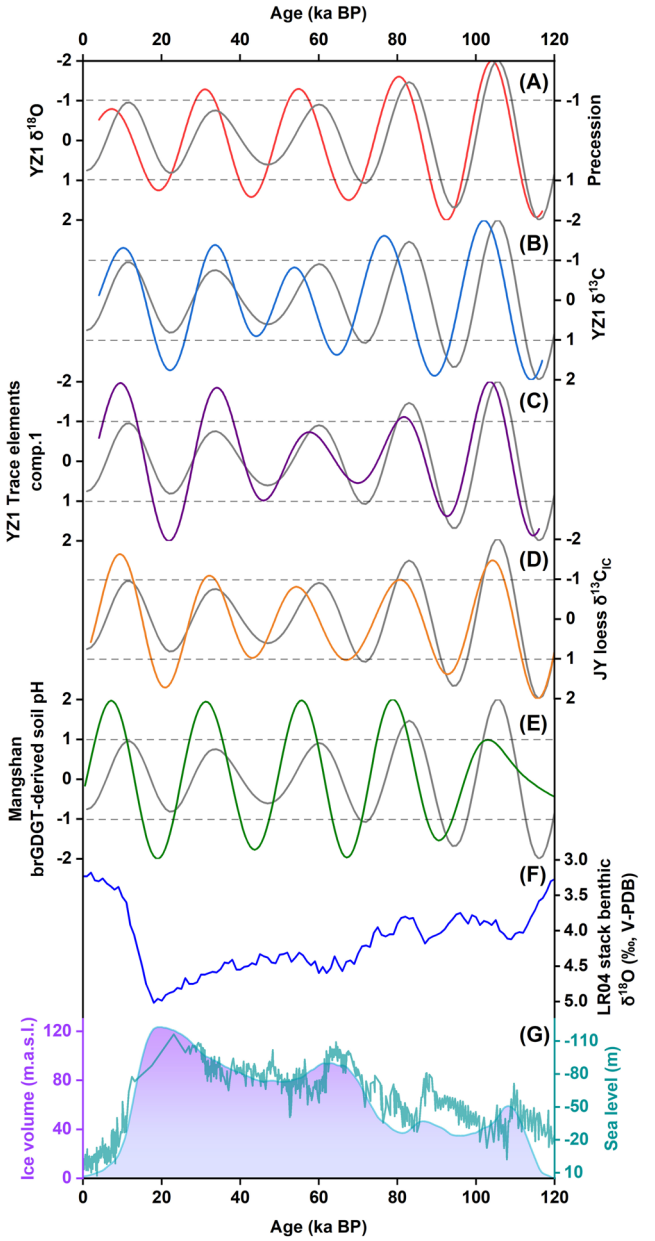

Figure 3. Influence of NHSI and ice sheet dynamics on ASM precipitation. (a–c) YZ1 $\delta^{18}O$,$\delta^{13}C$, and X/Ca PC1 records (this study); (d) The $\delta^{13}C$ of inorganic carbonate from the Chinese loess in northern China (Sun et al., 2019); (e) The brGDGT-derived soil pH for the Mangshan mountain (Peterse et al., 2014); (f) Global stack benthic foraminifer $\delta^{18}O$ sequence LR04 (Lisiecki & Raymo, 2005); (g) Global ice volume and sea level reconstructing records (Bintanja and van de Wal, 2008; Grant et al., 2014). The gray curve represents the variation in the precession. The frequency is 0.0434 ka^{-1} and the band width is 0.01 ka^{-1}, normalized to the interval −2 to 2.

The decrease in monsoon precipitation may be related to the large global ice volume during the LGM (Figure 3g). During the LGM, although the insolation decrease is minor compared to the MIS3, MIS4 and MIS5, the large-scale cooling of the NH continents due to the increased global ice volume produces high-pressure anomalies over Eurasia and low-pressure anomalies over the North Pacific, respectively, which further reduces the land-sea thermal contrast (Lyu et al., 2021; Tian & Jiang, 2016). Meanwhile, ocean cooling weakens local upward movement and air convection over the oceans, which leads to a weakening of the ASM and a reduction in ocean moisture fluxes. Strong cooling at NH high latitudes will lead to a strengthening and southward shift of NH subtropical westerlies, which limits the extent and intensity of summer monsoon penetrating deep into the East Asian continent (Chiang et al., 2020). On the other hand, the location of the ITCZ is sensitive to changes in ice volume in NH and the resulting differential heating between the two hemispheres (McGee et al., 2018). Thus, during the LGM, although the weakening of insolation is not significant, the large ice volume during this period amplified the magnitude of the reduction of monsoon precipitation. This feature has been captured in fully forced transient experiments (Lyu et al., 2021; Shi et al., 2019), which we verify from the reconstructed record.

Another period of significantly reduced precipitation was during end of MIS5e. Almost all records indicate that precipitation reduced to the extent of the LGM during end of MIS5e, although this time ice volumes were much smaller (Figure 3). Modeling work suggests that the relationship between ASM precipitation and ice volume is non-linear (Yin et al., 2009). Especially in the lower latitudes of 15°–25°N, precipitation does not entirely follow the change in ice volume, rainfall in southern China is less affected by ice volume in low insolation conditions (Lyu et al., 2021). Thus, forcing from ice volume is limited during end of MIS5e, and insolation dominates the monsoon precipitation variations.

The retreat of the coastline during the LGM resulted in an increase in the distance (100–300 km) from the study area to the ocean (Figure S9 in Supporting Information S1), lengthening the distance between the oceanic moisture source and the cave site. The continuous condensation of monsoonal moisture in the transport path reduces monsoonal precipitation reaching the inland. The more significant Rayleigh fractionation process during moisture transport due to the retreating coastline will result in more negative $\delta^{18}Op$ and thus $\delta^{18}Oc$ downstream. This offsets the effect of positive $\delta^{18}Op$ due to positive seawater $\delta^{18}O$ (~1.7‰) during the LGM (Schrag et al., 1996), resulting in insignificant variation in $\delta^{18}Op$ over central and eastern China (~1.0–2.0‰) (Cai et al., 2015). Consequently, the relative magnitude of $\delta^{18}O$ variations is smaller than the amplitude of the trace element-derived precipitation reconstruction during the LGM. Our previous results also show that the enriched $\delta^{18}Oc$ during MIS5d and end of MIS5e are attributed to the isotopic compositions of different moisture sources and the dynamics of the monsoon circulation (Wu et al., 2020). Therefore, we suggest that $\delta^{18}Oc$ primarily captures features of ASM dynamics, such as intensity, but caution is still advised when using it for precipitation reconstruction.

5. Conclusions

Based on high-resolution stalagmite trace element records, for the first time, we infer variations of the regional hydrological environment in southwest China during 4.07–116.09 ka BP. Our study highlights that the NHSI and differences in insolation in the interhemispheric tropics are the primary control on ASM precipitation phase

variations. However, global ice volume moderates the magnitude of the response of monsoonal precipitation amount to changes in insolation. We suggest that discussions of the meridional tripolar distribution pattern in monsoon region in China on the orbital scale should be carefully considered regarding the range of its influence, although this pattern is highly significant during the modern and last glacial millennial events. This study provides a robust reference for precipitation variations in monsoon region in China, which can be used to validate the paleo precipitation simulation data.

Conflict of Interest

The authors declare no conflicts of interest relevant to this study.

Data Availability Statement

All trace element data interpolated to isotopic resolution and LA-ICP-MS raw data is available at Wu, Warken, et al. (2023). Chronological and stable isotope data are available at Wu, Li, et al. (2023).

Acknowledgments
The analytical infrastructure at Institute of Environmental Physics was supported through the German Science Grant (No. 247825108) and a structure and innovation fund of the region of Baden Württemberg. Yao Wu received support through a grant by the China Scholarship Council (No. 202106990014). This research was also supported by the National Natural Science Foundation of China (NSFC, No. 42172204, 42272214, and 41888101), Yunnan Fundamental Research Projects (Grant 202201AS070022), the Young and Middle-age Academic and Technical Leader in Yunnan Province (No. 202205AC160025) to T.-Y Li. We are grateful to the editor and anonymous reviewers for their insightful comments, which have greatly improved the manuscript. For the publication fee we acknowledge financial support by DFG within the funding program "Open Access Publication Funding" as well as by Heidelberg University. Open Access funding enabled and organized by Projekt DEAL.

References

Beck, J. W., Zhou, W. J., Li, C., Wu, Z. K., White, L., Xian, F., et al. (2018). A 550,000-year record of East Asian monsoon rainfall from ^{10}Be in loess. *Science*, *360*(6391), 877–881. https://doi.org/10.1126/science.aam5825

Bintanja, R., & van de Wal, R. S. W. (2008). North American ice-sheet dynamics and the onset of 100,000-year glacial cycles. *Nature*, *454*(7206), 869–872. https://doi.org/10.1038/nature07158

Cai, Y. J., Fung, I. Y., Edwards, R. L., An, Z. S., Cheng, H., Lee, J.-E., et al. (2015). Variability of stalagmite-inferred Indian monsoon precipitation over the past 252,000 y. *Proceedings of the National Academy of Sciences of the United States of America*, *112*(10), 2954–2959. https://doi.org/10.1073/pnas.1424035112

Chen, J. S., Zhao, K., Wang, Y. J., Cui, Y. F., Liang, Y. J., Shao, Q. F., et al. (2022). ENSO effect on hydroclimate changes in southeastern China over the past two millennia. *Quaternary Science Reviews*, *285*, 107539. https://doi.org/10.1016/j.quascirev.2022.107539

Cheng, H., Edwards, R. L., Sinha, A., Spötl, C., Yi, L., Chen, S. T., et al. (2016). The Asian monsoon over the past 640,000 years and ice age terminations. *Nature*, *534*(7609), 640–646. https://doi.org/10.1038/nature18591

Cheng, H., Li, H. Y., Sha, L. J., Sinha, A., Shi, Z. G., Yin, Q. Z., et al. (2022). Milankovitch theory and monsoon. *The Innovation*, *3*(6), 100338. https://doi.org/10.1016/j.xinn.2022.100338

Cheng, H., Zhang, H. W., Cai, Y. J., Shi, Z. G., Yi, L., Deng, C. L., et al. (2021). Orbital-scale Asian summer monsoon variations: Paradox and exploration. *Science China Earth Sciences*, *64*(4), 529–544. https://doi.org/10.1007/s11430-020-9720-y

Cheng, H., Zhang, H. W., Zhao, J. Y., Li, H. Y., Ning, Y., & Kathayat, G. (2019). Chinese stalagmite paleoclimate researches: A review and perspective. *Science China Earth Sciences*, *62*(10), 1489–1513. https://doi.org/10.1007/s11430-019-9478-3

Chiang, J. C. H., Herman, M. J., Yoshimura, K., & Fung, I. Y. (2020). Enriched East Asian oxygen isotope of precipitation indicates reduced summer seasonality in regional climate and westerlies. *Proceedings of the National Academy of Sciences of the United States of America*, *117*(26), 14745–14750. https://doi.org/10.1073/pnas.1922602117

Chiang, J. C. H., Swenson, L. M., & Kong, W. (2017). Role of seasonal transitions and the westerlies in the interannual variability of the East Asian summer monsoon precipitation: Seasonal transitions in EASM variability. *Geophysical Research Letters*, *44*(8), 3788–3795. https://doi.org/10.1073/pnas.1922602117

Clemens, S. C., Holbourn, A., Kubota, Y., Lee, K. E., Liu, Z., Chen, G., et al. (2018). Precession-band variance missing from East Asian monsoon runoff. *Nature Communications*, *9*(1), 3364. https://doi.org/10.1038/s41467-018-05814-0

Dai, G. W., Zhang, Z. S., Otterå, O. H., Langebroek, P. M., Yan, Q., & Zhang, R. (2021). A modeling study of the tripole pattern of East China precipitation over the past 425 ka. *Journal of Geophysical Research: Atmospheres*, *126*(7), e2020JD033513. https://doi.org/10.1029/2020JD033513

Day, C. C., & Henderson, G. M. (2013). Controls on trace-element partitioning in cave-analogue calcite. *Geochimica et Cosmochimica Acta*, *120*, 612–627. https://doi.org/10.1016/j.gca.2013.05.044

Fairchild, I. J., Smith, C. L., Baker, A., Fuller, L., Spötl, C., Mattey, D., et al. (2006). Modification and preservation of environmental signals in speleothems. *Earth-Science Reviews*, *75*(1–4), 105–153. https://doi.org/10.1016/j.earscirev.2005.08.003

Fohlmeister, J., Voarintsoa, N. R. G., Lechleitner, F. A., Boyd, M., Brandtstätter, S., Jacobson, M. J. L., & L. Oster, J. (2020). Main controls on the stable carbon isotope composition of speleothems. *Geochimica et Cosmochimica Acta*, *279*, 67–87. https://doi.org/10.1016/j.gca.2020.03.042

Gabitov, R. I., Sadekov, A., & Leinweber, A. (2014). Crystal growth rate effect on Mg/Ca and Sr/Ca partitioning between calcite and fluid: An in situ approach. *Chemical Geology*, *367*, 70–82. https://doi.org/10.1016/j.chemgeo.2013.12.019

Grant, K. M., Rohling, E. J., Ramsey, C. B., Cheng, H., Edwards, R. L., Florindo, F., et al. (2014). Sea-level variability over five glacial cycles. *Nature Communications*, *5*(1), 5076. https://doi.org/10.1038/ncomms6076

Hu, C. Y., Henderson, G. M., Huang, J. H., Xie, S. C., Sun, Y., & Johnson, K. R. (2008). Quantification of Holocene Asian monsoon rainfall from spatially separated cave records. *Earth and Planetary Science Letters*, *266*(3–4), 221–232. https://doi.org/10.1016/j.epsl.2007.10.015

Jamieson, R. A., Baldini, J. U. L., Brett, M. J., Taylor, J., Ridley, H. E., Ottley, C. J., et al. (2016). Intra- and inter-annual uranium concentration variability in a Belizean stalagmite controlled by prior aragonite precipitation: A new tool for reconstructing hydro-climate using aragonitic speleothems. *Geochimica et Cosmochimica Acta*, *190*, 332–346. https://doi.org/10.1016/j.gca.2016.06.037

Jian, Z. M., Wang, Y., Dang, H. W., Mohtadi, M., Rosenthal, Y., Lea, D. W., et al. (2022). Warm pool ocean heat content regulates ocean–continent moisture transport. *Nature*, *612*(7938), 92–99. https://doi.org/10.1038/s41586-022-05302-y

Jiang, S. W., Zhou, X., Sachs, J. P., Luo, W. H., Tu, L. Y., Liu, X. Q., et al. (2021). Central eastern China hydrological changes and ENSO-like variability over the past 1800 yr. *Geology*, *49*(11), 1386–1390. https://doi.org/10.1130/G48894.1

Jochum, K. P., Weis, U., Stoll, B., Kuzmin, D., Yang, Q. C., Raczek, I., et al. (2011). Determination of reference values for NIST SRM 610–617 glasses following ISO guidelines. *Geostandards and Geoanalytical Research*, *35*(4), 397–429. https://doi.org/10.1111/j.1751-908X.2011.00120.x

Lachniet, M. S. (2020). Illuminating the meaning of Asian monsoon cave speleothem records. *Paleoceanography and Paleoclimatology*, *35*(1), e2019PA003841. https://doi.org/10.1029/2019PA003841

Laskar, J., Robutel, P., Joutel, F., Gastineau, M., Correia, A. C. M., & Levrard, B. (2004). A long-term numerical solution for the insolation quantities of the Earth. *Astronomy & Astrophysics*, *428*(1), 261–285. https://doi.org/10.1051/0004-6361:20041335

Li, N. N., Sharifi, A., Chambers, F. M., Ge, Y., Dubois, N., Gao, G. Z., et al. (2021). Linking Holocene East Asian monsoon variability to solar forcing and ENSO activity: Multi-proxy evidence from a peatland in Northeastern China. *The Holocene*, *31*(6), 966–982. https://doi.org/10.1177/0959683621994662

Li, Y. X., Rao, Z. G., Xu, Q. H., Zhang, S. R., Liu, X. K., Wang, Z. L., et al. (2020). Inter-relationship and environmental significance of stalagmite $\delta^{13}C$ and $\delta^{18}O$ records from Zhenzhu Cave, north China, over the last 130 ka. *Earth and Planetary Science Letters*, *536*, 116149. https://doi.org/10.1016/j.epsl.2020.116149

Lisiecki, L. E., & Raymo, M. E. (2005). A Pliocene-Pleistocene stack of 57 globally distributed benthic $\delta^{18}O$ records. *Paleoceanography*, *20*(1), PA1003. https://doi.org/10.1029/2004PA001071

Liu, D. B., Mi, X., Liu, S. S., & Wang, Y. J. (2022). Multi-phased Asian hydroclimate variability during Heinrich stadial 5. *Climate Dynamics*, *60*(11–12), 4003–4016. https://doi.org/10.1007/s00382-022-06566-w

Liu, J. H., Zhang, P. Z., Cheng, H., Chen, F. H., Yang, X. L., Zhang, D. Z., et al. (2008). Asian summer monsoon precipitation recorded by stalagmite oxygen isotopic composition in the western Loess Plateau during AD1875–2003 and its linkage with ocean-atmosphere system. *Chinese Science Bulletin*, *53*(13), 2041–2049. https://doi.org/10.1007/s11434-008-0286-5

Liu, X. K., Liu, J. B., Chen, S. Q., Chen, J. H., Zhang, X., Yan, J. J., & Chen, F. (2020). New insights on Chinese cave $\delta^{18}O$ records and their paleoclimatic significance. *Earth-Science Reviews*, *207*, 103216. https://doi.org/10.1016/j.earscirev.2020.103216

Liu, Z. Y., Wen, X. Y., Brady, E. C., Otto-Bliesner, B., Yu, G., Lu, H. Y., et al. (2014). Chinese cave records and the East Asia summer monsoon. *Quaternary Science Reviews*, *83*, 115–128. https://doi.org/10.1016/j.quascirev.2013.10.021

Lu, Z. Y., Liu, Z. Y., Chen, G. S., & Guan, J. (2019). Prominent precession band variance in enso intensity over the last 300,000 years. *Geophysical Research Letters*, *46*(16), 9786–9795. https://doi.org/10.1029/2019gl083410

Lyu, A. Q., Yin, Q. Z., Crucifix, M., & Sun, Y. B. (2021). Diverse regional sensitivity of summer precipitation in East Asia to ice volume, CO_2 and astronomical forcing. *Geophysical Research Letters*, *48*(7), e2020GL092005. https://doi.org/10.1029/2020GL092005

Maher, B. A., & Thompson, R. (2012). Oxygen isotopes from Chinese caves: Records not of monsoon rainfall but of circulation regime. *Journal of Quaternary Science*, *27*(6), 615–624. https://doi.org/10.1002/jqs.2553

McGee, D., Moreno-Chamarro, E., Green, B., Marshall, J., Galbraith, E., & Bradtmiller, L. (2018). Hemispherically asymmetric trade wind changes as signatures of past ITCZ shifts. *Quaternary Science Reviews*, *180*, 214–228. https://doi.org/10.1016/j.quascirev.2017.11.020

Miao, Y. F., Zhang, P., Lu, S. M., Wu, X. Y., Li, L. L., Chen, H. G., et al. (2015). Late quaternary pollen records from the Yangtze River Delta, East China, and its implications for the Asian monsoon evolution. *Arabian Journal of Geosciences*, *8*(10), 7845–7854. https://doi.org/10.1007/s12517-015-1777-8

Peterse, F., Martínez-García, A., Zhou, B., Beets, C. J., Prins, M. A., Zheng, H., & Eglinton, T. I. (2014). Molecular records of continental air temperature and monsoon precipitation variability in East Asia spanning the past 130,000 years. *Quaternary Science Reviews*, *83*, 76–82. https://doi.org/10.1016/j.quascirev.2013.11.001

Pu, J. B., Wang, A. Y., Yin, J. J., Shen, L. C., Sun, Y. C., Yuan, D. X., & Zhao, H. (2015). Processes controlling dripwater hydrochemistry variations in Xueyu cave, SW China: Implications for speleothem palaeoclimate signal interpretations. *Boreas*, *44*(3), 603–617. https://doi.org/10.1111/bor.12117

Ruan, J. Y., Zhang, H. Y., Cai, Z. Y., Yang, X. Q., & Yin, J. (2019). Regional controls on daily to interannual variations of precipitation isotope ratios in Southeast China: Implications for paleomonsoon reconstruction. *Earth and Planetary Science Letters*, *527*, 115794. https://doi.org/10.1016/j.epsl.2019.115794

Schrag, D. P., Hampt, G., & Murray, D. W. (1996). Pore fluid constraints on the temperature and oxygen isotopic composition of the glacial ocean. *Science*, *272*(5270), 1930–1932. https://doi.org/10.1126/science.272.5270.1930

Shi, X., Yang, Y., Cheng, H., Zhao, J. Y., Li, T.-Y., Lei, L. D., et al. (2022). Influences on Asian summer monsoon during Dansgaard-Oeschger events 19 to 25 (70–115 kyr B.P.). *Palaeogeography, Palaeoclimatology, Palaeoecology*, *587*, 110798. https://doi.org/10.1016/j.palaeo.2021.110798

Shi, Z. G., Xie, X. N., Ren, X., Li, X. Z., Yang, L., Lei, J., et al. (2019). Radiative effect of mineral Dust on East Asian summer monsoon during the last glacial maximum: Role of snow-Albedo feedback. *Geophysical Research Letters*, *46*(19), 10901–10909. https://doi.org/10.1029/2019GL084211

Sinclair, D. J., Banner, J. L., Taylor, F. W., Partin, J., Jenson, J., Mylroie, J., et al. (2012). Magnesium and strontium systematics in tropical speleothems from the Western Pacific. *Chemical Geology*, *294–295*, 1–17. https://doi.org/10.1016/j.chemgeo.2011.10.008

Stoll, H. M., Day, C., Lechleitner, F., Kost, O., Endres, L., Sliwinski, J., et al. (2022). Distinguishing the vegetation and soil component of $\delta^{13}C$ variation in speleothem records from degassing and prior calcite precipitation effects. *Climate of the Past Discussions*, *2022*, 1–30. https://doi.org/10.5194/cp-2022-77

Sun, Y. B., Kutzbach, J., An, Z. S., Clemens, S., Liu, Z. Y., Liu, W. G., et al. (2015). Astronomical and glacial forcing of East Asian summer monsoon variability. *Quaternary Science Reviews*, *115*, 132–142. https://doi.org/10.1016/j.quascirev.2015.03.009

Sun, Y. B., Yin, Q. Z., Crucifix, M., Clemens, S. C., Araya-Melo, P., Liu, W. G., et al. (2019). Diverse manifestations of the mid-Pleistocene climate transition. *Nature Communications*, *10*(1), 352. https://doi.org/10.1038/s41467-018-08257-9

Tan, L. C., An, Z. S., Huh, C.-A., Cai, Y. J., Shen, C.-C., Shiau, L.-J., et al. (2014). Cyclic precipitation variation on the western Loess Plateau of China during the past four centuries. *Scientific Reports*, *4*(1), 6381. https://doi.org/10.1038/srep06381

Tan, L. C., Cai, Y. J., Cheng, H., Lawrence Edwards, R., Shen, C.-C., Gao, Y. L., & An, Z. S. (2015). Climate significance of speleothem $\delta^{18}O$ from central China on decadal timescale. *Journal of Asian Earth Sciences*, *106*, 150–155. https://doi.org/10.1016/j.jseaes.2015.03.008

Tan, M. (2014). Circulation effect: Response of precipitation $\delta^{18}O$ to the ENSO cycle in monsoon regions of China. *Climate Dynamics*, *42*(3–4), 1067–1077. https://doi.org/10.1007/s00382-013-1732-x

Thomas, E. K., Clemens, S. C., Sun, Y., Prell, W. L., Huang, Y. S., Gao, L., et al. (2016). Heterodynes dominate precipitation isotopes in the East Asian monsoon region, reflecting interaction of multiple climate factors. *Earth and Planetary Science Letters*, *455*, 196–206. https://doi.org/10.1016/j.epsl.2016.09.044

Tian, S. H., Dai, G. W., Yin, Q. Z., Meng, X. Q., Zhang, Z. S., Zhu, Z. M., & Xiao, G. Q. (2022). Spatial differences in East Asian climate transition at ~260 ka and their links to ENSO. *Quaternary Science Reviews*, *296*, 107805. https://doi.org/10.1016/j.quascirev.2022.107805

Tian, Z. P., & Jiang, D. B. (2016). Revisiting last glacial maximum climate over China and East Asian monsoon using PMIP3 simulations. *Palaeogeography, Palaeoclimatology, Palaeoecology*, *453*, 115–126. https://doi.org/10.1016/j.palaeo.2016.04.020

Tremaine, D. M., & Froelich, P. N. (2013). Speleothem trace element signatures: A hydrologic geochemical study of modern cave dripwaters and farmed calcite. *Geochimica et Cosmochimica Acta*, *121*, 522–545. https://doi.org/10.1016/j.gca.2013.07.026

Wang, M., Chen, S. T., Wang, Y. J., Zhao, K., Wang, X. F., Liang, Y. J., et al. (2022). Stalagmite multi-proxy evidence of wet and dry intervals in the middle Yangtze Valley during the last glacial period. *Palaeogeography, Palaeoclimatology, Palaeoecology*, *586*, 110764. https://doi.org/10.1016/j.palaeo.2021.110764

Wang, Y., Lu, H. Y., Yi, S. W., Huber, M., Yang, F., Gu, Y., et al. (2022). Tropical forcing orbital-scale precipitation variations revealed by a maar lake record in South China. *Climate Dynamics*, *58*(9–10), 2269–2280. https://doi.org/10.1007/s00382-021-06004-3

Wang, Y. J., Cheng, H., Edwards, R. L., An, Z. S., Wu, J. Y., Shen, C. C., & Dorale, J. A. (2001). A high-resolution absolute-dated late pleistocene monsoon record from Hulu Cave, China. *Science*, *294*(5550), 2345–2348. https://doi.org/10.1126/science.1064618

Warken, S. F., Fohlmeister, J., Schröder-Ritzrau, A., Constantin, S., Spötl, C., Gerdes, A., et al. (2018). Reconstruction of late Holocene autumn/winter precipitation variability in SW Romania from a high-resolution speleothem trace element record. *Earth and Planetary Science Letters*, *499*, 122–133. https://doi.org/10.1016/j.epsl.2018.07.027

Warken, S. F., Schorndorf, N., Stinnesbeck, W., Hennhoefer, D., Stinnesbeck, S. R., Förstel, J., et al. (2021). Solar forcing of early Holocene droughts on the Yucatán peninsula. *Scientific Reports*, *11*(1), 13885. https://doi.org/10.1038/s41598-021-93417-z

Wassenburg, J. A., Riechelmann, S., Schröder-Ritzrau, A., Riechelmann, D. F. C., Richter, D. K., Immenhauser, A., et al. (2020). Calcite Mg and Sr partition coefficients in cave environments: Implications for interpreting prior calcite precipitation in speleothems. *Geochimica et Cosmochimica Acta*, *269*, 581–596. https://doi.org/10.1016/j.gca.2019.11.011

Wu, Y., Li, T.-Y., Li, J.-Y., Cheng, H., Ning, Y.-F., Shen, C.-C., et al. (2023). Variations in Asian summer monsoon and hydroclimate during Heinrich stadials 4 revealed by stalagmite stable isotopes and trace elements. *Quaternary Science Reviews*, *299*, 107869. https://doi.org/10.1016/j.quascirev.2022.107869

Wu, Y., Li, T.-Y., Yu, T.-L., Shen, C.-C., Chen, C.-J., Zhang, J., et al. (2020). Variation of the Asian summer monsoon since the last glacial-interglacial recorded in a stalagmite from southwest China. *Quaternary Science Reviews*, *234*, 106261. https://doi.org/10.1016/j.quascirev.2020.106261

Wu, Y., Li, T.-Y., Yu, T.-L., Shen, C.-C., Zhang, J., Li, J.-Y., et al. (2023). Variation of the Asian summer monsoon since the last glacial-interglacial recorded in a stalagmite from southwest China [Dataset]. Zenodo. https://doi.org/10.5281/zenodo.8264200

Wu, Y., Warken, S., Frank, N., Mielke, A., Chen, C.-J., Li, J.-Y., & Li, T.-Y. (2023). Northern Hemisphere summer insolation and ice volume driven variations in hydrological environment in southwest China [Dataset]. Zenodo. https://doi.org/10.5281/zenodo.10072475

Xue, Y.-X., Zhang, J., Su, Z., Wu, Y., Liang, Q.-S., Liang, M.-Q., et al. (2023). Quantifying source effects based on rainwater $\delta^{18}O$ from 10-year monitoring records in Southwest China. *Applied Geochemistry*, *155*, 105706. https://doi.org/10.1016/j.apgeochem.2023.105706

Yang, Y., Yang, R. W., Cao, J., Zhao, J. Y., Cheng, H., & Wang, J. (2019). Relationship between the Asian summer monsoon circulation and speleothem $\delta^{18}O$ of Xiaobailong cave. *Climate Dynamics*, *53*(9–10), 6351–6362. https://doi.org/10.1007/s00382-019-04935-6

Yin, Q. Z., Berger, A., & Crucifix, M. (2009). Individual and combined effects of ice sheets and precession on MIS-13 climate. *Climate of the Past*, *5*(2), 229–243. https://doi.org/10.5194/cp-5-229-2009

Zhang, H. B., Griffiths, M. L., Chiang, J. C. H., Kong, W. W., Wu, S. T., Atwood, A., et al. (2018). East Asian hydroclimate modulated by the position of the westerlies during Termination I. *Science*, *362*(6414), 580–583. https://doi.org/10.1126/science.aat9393

Zhang, J. P., Lu, H. Y., Jia, J. W., Shen, C. M., Wang, S. Y., Chu, G. Q., et al. (2020). Seasonal drought events in tropical East Asia over the last 60,000 y. *Proceedings of the National Academy of Sciences of the United States of America*, *117*(49), 30988–30992. https://doi.org/10.1073/pnas.2013802117

Zhang, X., Zheng, Z., Huang, K. Y., Cheng, J., Cheddadi, R., Zhao, Y., et al. (2023). Quantification of Asian monsoon variability from 68 ka BP through pollen-based climate reconstruction. *Science Bulletin*, *68*(7), 713–722. https://doi.org/10.1016/j.scib.2023.03.013

Zhao, D. B., Lu, Z. Y., Wan, S. M., Cheng, H., Shi, X. F., & Li, A. C. (2023). Quaternary rainfall variability is governed by insolation in northern China and ice-sheet forcing in the South. *Communications Earth & Environment*, *4*(1), 7. https://doi.org/10.1038/s43247-022-00670-9

Zhao, J. Y., Cheng, H., Cao, J., Sinha, A., Dong, X. Y., Pan, L. K., et al. (2023). Orchestrated decline of Asian summer monsoon and Atlantic meridional overturning circulation in global warming period. *The Innovation: Geoscience*, *1*(1), 100011. https://doi.org/10.59717/j.xinn-geo.2023.100011

Zhu, X. W., Zhang, Y. H., Han, D. S., Wen, R. P., & Chen, B. Q. (2004). Cave characteristics and speleothems in Xueyu cave group, Fengdu, Chongqing city (in Chinese). *Carsologica Sinica*, *23*, 85–90. https://doi.org/10.3969/j.issn.1001-4810.2004.02.001

References From the Supporting Information

Dawson, A. (2016). eofs: A Library for EOF analysis of meteorological, oceanographic, and climate data. *Journal of Open Research Software*, *4*(1), e14. https://doi.org/10.5334/jors.122

De Groeve, J., Kusumoto, B., Koene, E., Kissling, W. D., Seijmonsbergen, A. C., Hoeksema, B. W., et al. (2022). Global raster dataset on historical coastline positions and shelf sea extents since the Last Glacial Maximum. *Global Ecology and Biogeography*, *31*(11), 2162–2171. https://doi.org/10.1111/geb.13573

Kalnay, E., Kanamitsu, M., Kistler, R., Collins, W., Deaven, D., Gandin, L., et al. (1996). The NCEP/NCAR 40-year reanalysis project. *Bulletin of the American Meteorological Society*, *77*(3), 437–472. https://doi.org/10.1175/1520-0477(1996)077<0437:TNYRP>2.0.CO;2

Lea, D. W., Pak, D. K., & Spero, H. J. (2000). Climate impact of late quaternary equatorial Pacific Sea surface temperature variations. *Science*, *289*(5485), 1719–1724. https://doi.org/10.1126/science.289.5485.1719

Scholz, D., & Hoffmann, D. L. (2011). StalAge—An algorithm designed for construction of speleothem age models. *Quaternary Geochronology*, *6*(3), 369–382. https://doi.org/10.1016/j.quageo.2011.02.002

Wu, Z. H., & Huang, N. E. (2009). Ensemble empirical mode decomposition: A noise assisted data analysis method. *Advances in Adaptive Data Analysis*, *1*(01), 1–41. https://doi.org/10.1142/S1793536909000047

Yatagai, A., Kamiguchi, K., Arakawa, O., Hamada, A., Yasutomi, N., & Kitoh, A. (2012). APHRODITE: Constructing a long-term daily gridded precipitation dataset for Asia based on a dense network of rain gauges. *Bulletin of the American Meteorological Society*, *93*(9), 1401–1415. https://doi.org/10.1175/BAMS-D-11-00122.1

Zhang, S., Li, T. G., Chang, F. M., Yu, Z. F., Xiong, Z. F., & Wang, H. X. (2017). Correspondence between the ENSO-like state and glacial-interglacial condition during the past 360 kyr. *Chinese Journal of Oceanology and Limnology*, *35*(5), 1018–1031. https://doi.org/10.1007/s00343-017-6082-9

Zhang, S., Yu, Z. F., Gong, X., Wang, Y., Chang, F. M., Lohmman, G., et al. (2021). Precession cycles of the El Niño/Southern oscillation-like system controlled by Pacific upper-ocean stratification. *Communications Earth & Environment*, *2*(1), 239. https://doi.org/10.1038/s43247-021-00305-5